nature neuroscience

ARTICLES

A population of Nestin-expressing progenitors in the cerebellum exhibits increased tumorigenicity

Peng Li[1,2], Fang Du[1], Larra W Yuelling[1], Tiffany Lin[3], Renata E Muradimova[1], Rossella Tricarico[1], Jun Wang[4], Grigori Enikolopov[5], Alfonso Bellacosa[1], Robert J Wechsler-Reya[3,4] & Zeng-jie Yang[1]

It is generally believed that cerebellar granule neurons originate exclusively from granule neuron precursors (GNPs) in the external germinal layer (EGL). Here we identified a rare population of neuronal progenitors in mouse developing cerebellum that expresses Nestin. Although Nestin is widely considered a marker for multipotent stem cells, these Nestin-expressing progenitors (NEPs) are committed to the granule neuron lineage. Unlike conventional GNPs, which reside in the outer EGL and proliferate extensively, NEPs reside in the deep part of the EGL and are quiescent. Expression profiling revealed that NEPs are distinct from GNPs and, in particular, express markedly reduced levels of genes associated with DNA repair. Consistent with this, upon aberrant activation of Sonic hedgehog (Shh) signaling, NEPs exhibited more severe genomic instability and gave rise to tumors more efficiently than GNPs. These studies revealed a previously unidentified progenitor for cerebellar granule neurons and a cell of origin for medulloblastoma.

Nestin, a type IV intermediate filament protein, was first identified in multipotent neural stem cells (NSCs)[1]. Since then, Nestin has been widely used as a marker for NSCs in various regions of the nervous system. It is generally believed that as NSCs differentiate into lineage-restricted progenitors, Nestin is replaced by neurofilament and glial fibrillary acidic protein (GFAP) in neurons and glial cells, respectively[2]. These events may reflect temporal and spatial control of intermediate filament expression, which facilitates changes in cellular shape and migratory potential. However, several studies have suggested that not all Nestin-expressing cells are NSCs and that some are lineage-committed neuronal and glial progenitors[3,4]. Furthermore, recent studies have suggested that Nestin expression is not limited to the nervous system: for example, Nestin$^+$ cells have been described in the skin, pancreas and kidney[5]. These studies suggest that Nestin cannot be unambiguously interpreted as a marker for NSCs.

In the cerebellum, Nestin expression has been well-documented in both NSCs and radial (Bergmann) glia[6–9]. However, Nestin expression in GNPs has been controversial: whereas some reports have suggested that Nestin expression is extinguished before cells commit to the granule lineage[10], others have suggested that GNPs can express Nestin[11–13]. In part, these discrepancies may be due to the fact that the EGL, where GNPs reside, is traversed by the processes of Bergmann glia, making it difficult to distinguish Nestin$^+$ cells from Nestin$^+$ fibers. In many studies, animals that express Cre recombinase under the control of the nestin promoter have been used to target GNPs[14,15]. However, it is not known whether recombination occurs in GNPs themselves or in the NSCs that give rise to them.

In this study, we identified a population of progenitors in the developing cerebellum that express high levels of Nestin. Despite lacking the canonical GNP lineage marker Math1 (encoded by *Atoh1*, here referred to as *Math1*), these NEPs are committed to the granule neuron lineage. NEPs are distinct from conventional GNPs in terms of location, proliferative status and gene expression. In particular, genes associated with DNA repair are underexpressed in NEPs compared with GNPs. After activation of Shh signaling, NEPs exhibit more severe genomic instability and give rise to medulloblastoma more efficiently than GNPs. Our studies therefore revealed a unique population of neuronal progenitors in the developing cerebellum and suggest that the intrinsic properties of the cell of origin can serve as predisposing factors for tumorigenesis.

RESULTS

A rare cell population in cerebellar EGL expresses Nestin

In the cerebellum, Nestin expression has been well-described in both NSCs and Bergmann glia[6–9]. However, whether GNPs express Nestin still remains unresolved.

To evaluate Nestin expression in the developing cerebellum, we first performed immunohistochemical staining using antibodies to Nestin. We readily detected Nestin protein in the cerebellum of mice at postnatal day 4 (P4; **Fig. 1a**). However, because Nestin protein is distributed both in the cytoplasm and on cell fibers, it is difficult to clearly distinguish Nestin-expressing cells based on immunostaining. To circumvent this limitation, we used *Nestin-CFP* transgenic mice, which express a nuclear-localized form of CFP driven by the

[1]Cancer Biology Program, Fox Chase Cancer Center, Temple University Health System, Philadelphia, Pennsylvania, USA. [2]Department of Clinical Biochemistry, Southwest Hospital, Third Military Medical University, Chongqing, China. [3]Department of Pharmacology and Cancer Biology, Duke University Medical Center, Durham, North Carolina, USA. [4]Tumor Initiation and Maintenance Program, National Cancer Institute–Designated Cancer Center, Sanford-Burnham Medical Research Institute, La Jolla, California, USA. [5]Cold Spring Harbor Laboratory, Cold Spring Harbor, New York, USA. Correspondence should be addressed to R.J.W.-R. (rwreya@sanfordburnham.org) and Z.Y. (zengjie.yang@fccc.edu).

Received 15 April; accepted 13 September; published online 20 October 2013; doi:10.1038/nn.3553

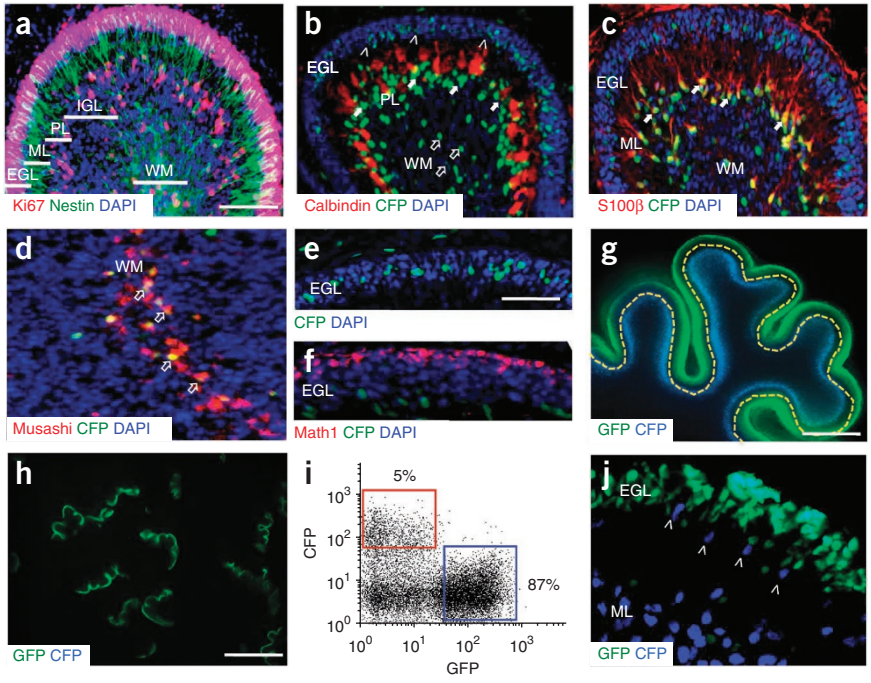

Figure 1 Identification and purification of NEPs in the developing cerebellum. (**a**) Cerebellar section from a wild-type mouse at P4, immunostained with antibodies to Nestin and Ki67. Horizontal white lines mark different cell layers in the cerebellum. PL, Purkinje layer; ML, molecular layer; WM, white matter. (**b**–**f**) Sections from cerebellum of a P4 *Nestin-CFP* mouse, stained with antibodies to CFP (**b**–**f**), Calbindin (**b**), S100β (**c**), Musashi (**d**) and Math1 (**f**). CFP$^+$ cells are marked in the EGL (arrowheads), the molecular layer (filled arrows) and the white matter (unfilled arrows). Sections in **a**–**f** were counterstained with DAPI (blue). (**g**,**h**) Fluorescence micrographs of cerebellar slices freshly prepared from *Math1-GFP–Nestin-CFP* animals at P4 (**g**; microdissected along the yellow dashed line) and dissected EGLs (**h**; collected for tissue dissociation). (**i**) Flow cytometry analysis of cells harvested from dissociated EGLs shown in **h**. Percentage indicates the proportion of GFP$^+$ cells and CFP$^+$ cells. (**j**) Confocal microscopy image of a cerebellar section prepared from *Math1-GFP–Nestin-CFP* mouse at P4 (GFP, green; CFP, blue). NEPs (arrowheads) were distinct from GFP$^+$ GNPs. Scale bars, 200 μm (**a**–**d**); 100 μm (**e**,**f**,**j**); 400 μm (**g**); and 2 mm (**h**).

promoter and second intron of the nestin gene[16]. This protein does not label fibers and therefore makes it easy to identify the cell bodies of Nestin-expressing cells. In the cerebellum of *Nestin-CFP* mice at P4, at least three populations of cells were CFP$^+$ (**Fig. 1b**). Consistent with previous reports[6,8], CFP$^+$ cells included Bergmann glia in the molecular layer (S100β$^+$, **Fig. 1c**) and NSCs in the white matter (Musashi$^+$, **Fig. 1d**). In addition, a small population of cells in the EGL expressed the *Nestin-CFP* transgene (**Fig. 1e**). All the CFP$^+$ cells in the EGL (NEPs) did not express Math1 (**Fig. 1f**), a well-characterized marker for GNPs[17]. In addition, Math1$^+$ GNPs resided in the superficial part of the EGL, whereas NEPs were predominantly localized in the deep EGL of the developing cerebellum (**Fig. 1f**). These data suggest that NEPs may be a previously unidentified cell population that is distinct from conventional GNPs. In *Nestin-CFP* transgenic mice, we found NEPs only in the cerebellum during early development (E16.5–P15). At embryonic day 14.5 (E14.5), we detected no Nestin-expressing cells in the EGL (**Supplementary Fig. 1a**) or in the rhombic lip (**Supplementary Fig. 1b**) where GNPs originate[10]. We first detected NEPs in the EGL at E16.5 (**Supplementary Fig. 1c**,**d**) and we did not find them in the postnatal cerebellum at P21 (**Supplementary Fig. 1e**). These data indicate that NEPs are a transient population that exists only during early cerebellar development.

To further characterize NEPs in the EGL, we purified these cells. For this purpose, we crossed *Nestin-CFP* mice with *Math1-GFP* mice, in which conventional GNPs exclusively express GFP[18]. We then prepared sagittal cerebellar slices from P4 *Math1-GFP–Nestin-CFP* mice, and microdissected cerebellar EGLs under a fluorescence microscope to exclude the Nestin$^+$ cells in the molecular layer and the white matter (**Fig. 1g**). We dissociated the dissected EGLs (**Fig. 1h**) and analyzed them by flow cytometry to detect expression of GFP and CFP. The majority of cells in the EGL were GFP$^+$ (**Fig. 1i**), indicating that cerebellar EGL is dominated by Math1$^+$ GNPs. Approximately 3–5% of cells in the EGL expressed *Nestin-CFP*, which is consistent with our immunohistochemical staining of cerebellar sections (**Fig. 1b**). Almost none of the cells were both GFP$^+$ and CFP$^+$ based on the flow cytometric analysis (**Fig. 1i**). Using confocal microscopy, we confirmed that GFP$^+$ GNPs and CFP$^+$ NEPs were mutually exclusive in the EGL of *Math1-GFP–Nestin-CFP* mice at P4 (**Fig. 1j**). These data suggest that NEPs and GNPs are two distinct cell populations in the postnatal EGL. As a control, we also dissected the white matter from the cerebellum of *Math1-GFP–Nestin-CFP* mice (**Supplementary Fig. 2a**,**b**). FACS analysis (**Supplementary Fig. 2c**–**e**) indicated that more than 18% of cells in the white matter were CFP$^+$, and 35% of CFP$^+$ cells expressed Prominin1, a marker for NSCs[19], suggesting that at least some of the Nestin-expressing cells in the white matter are NSCs.

To determine whether the CFP and GFP fluorescence in the cerebellum of *Nestin-CFP–Math1-GFP* mice faithfully reflects expression of endogenous Nestin and Math1 proteins, we examined FACS-sorted CFP$^+$ cells and GFP$^+$ cells by immunocytochemistry. All GFP$^+$ cells isolated from the EGL in *Nestin-CFP–Math1-GFP* animals at P4 were Math1$^+$ but lacked Nestin protein (**Supplementary Fig. 3a**–**d**). Similarly, we detected Nestin protein in the cytoplasm of all sorted CFP$^+$ cells, which lacked Math1 protein (**Supplementary Fig. 3e**–**h**). These data suggest that NEPs and GNPs can be purified from cerebellum of *Nestin-CFP–Math1-GFP* mice by microdissection followed by FACS.

NEPs are committed to the granule neuron lineage

As Nestin is commonly used as a marker for NSCs, we examined whether NEPs isolated from the EGL might represent NSCs. NSCs from many parts of the central nervous system proliferate and form macroscopic neurospheres when cultured in the presence of growth factors such as epidermal growth factor (EGF) and basic fibroblast growth factor (bFGF)[20]. To examine the capacity of NEPs to form neurospheres in culture, we purified NEPs and GNPs from the EGL of the cerebellum P4 *Nestin-CFP–Math1-GFP* mice and cultured them at clonal density in the presence of bFGF and EGF. As controls, we also cultured NSCs (Prominin1$^+$Lin$^-$ cells) isolated from the same cerebellum as previously described[6]. After 7 d, neurospheres were readily detectable in cultures of NSCs, whereas almost no neurospheres were generated from NEPs and GNPs (**Fig. 2a**,**b**). These data indicate that unlike NSCs, NEPs have a limited capacity to form neurospheres *in vitro*.

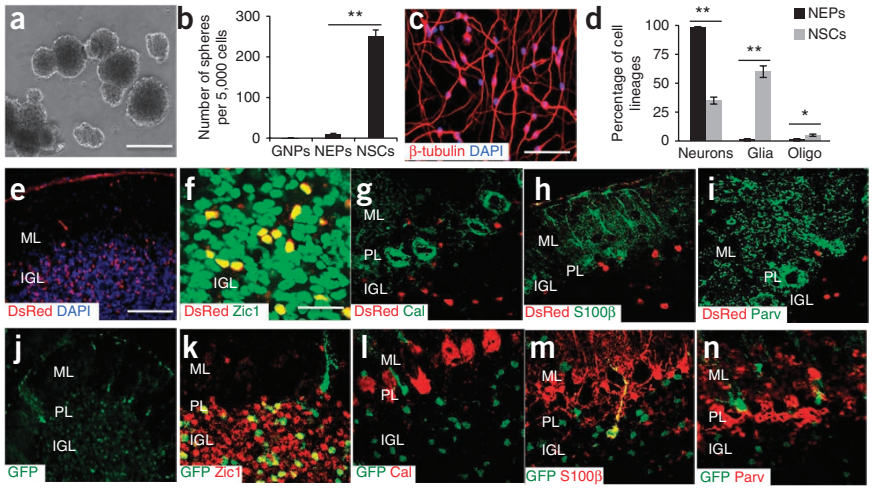

Figure 2 Neuronal lineage commitment of NEPs *in vivo* and *in vitro*. (**a**) Phase contrast image of neurospheres generated from NSC culture in the presence of EGF and bFGF. (**b**) Number of neurospheres per 5,000 NSCs, GNPs and NEPs after 7 d in culture under stem cell culture conditions. (**c**) After 4 d under differentiation conditions, NEPs were stained for β-tubulin (red) and counterstained with DAPI (blue). (**d**) Percentage of neurons (β-tubulin$^+$), Bergmann glia (S100β$^+$) and oligodendrocytes (O4$^+$) was quantified after culturing NSCs and NEPs under differentiation culture conditions. NEPs exclusively differentiate into neurons *in vitro*. (**e**–**i**) NEPs isolated from P4 *Nestin-CFP–DsRed* animals were transplanted into the cerebellum of P4 SCID mice. At P21, the recipient cerebellum was sectioned and immunostained with the indicated antibodies. NEPs gave rise to only neurons after the transplantation. (**j**–**n**) Cerebellar sections from *Nestin-CreER^{T2}–R26R-GFP* animals at P21 were immunostained with the indicated antibodies. PL, Purkinje layer; ML, molecular layer. Error bars (**b**,**d**), s.e.m. ($n = 3$). $^{**}P < 0.01$ and $^{*}P < 0.05$ (two-tailed Student's t test); NEPs versus NSCs in **b**, $P = 0.0015$, $df = 2$; neurons derived from NEPs versus NSCs in **d**, $P = 0.00461$; glia derived from NEPs versus NSCs in **d**, $P = 0.00431$; oligodendrocytes derived from NEPs versus NSCs in **d**, $P = 0.0153$. Scale bars, 2 mm (**a**); 200 μm (**c**,**e**,**j**); and 67 μm (**f**; same scale in **g**–**i**,**k**–**n**).

Another important characteristic of NSCs is their capability to differentiate into multiple cell lineages including neurons, astrocytes and oligodendrocytes[20]. To examine whether NEPs exhibit multipotency, we cultured purified NEPs and NSCs under differentiation culture conditions. After 3 d *in vitro*, NSCs differentiated into neurons (βIII-tubulin$^+$), astrocytes (S100β$^+$) and oligodendrocytes (O4$^+$) (**Supplementary Fig. 4**). In contrast, NEPs exclusively gave rise to βIII-tubulin$^+$ neurons (**Fig. 2c**). Fewer than 2% of cells in NEP cultures were Bergmann glia or oligodendrocytes (**Fig. 2d**). These data suggest that NEPs represent lineage-restricted neuronal progenitors rather than multipotent stem cells.

To confirm the neuronal lineage commitment of NEPs, we examined their differentiation potential *in vivo* using intracranial transplantation assays. We purified NEPs from the EGL of P4 *Nestin-CFP–Actin-DsRed* animals (which express red fluorescent protein in all cells[21]), and then transplanted them into the cerebellum of strain CB17 severe combined immunodeficient (SCID) animals at P4. We detected no proliferation among NEPs after the transplantation based the immunohistochemical staining for Ki67 (data not shown). At P21, we sectioned recipient cerebella to detect the differentiation of transplanted cells (DsRed$^+$, **Fig. 2e**). All DsRed$^+$ cells were Zic1$^+$ (**Fig. 2f**), a marker of cerebellar granule neurons[22], and in the recipient cerebellum we found no DsRed$^+$ Purkinje neurons (Calbindin$^+$, **Fig. 2g**), Bergmann glial cells (S100β$^+$, **Fig. 2h**) or interneurons (Parvalbumin$^+$, **Fig. 2i**). As a comparison, NSCs (Prominin1$^+$Lin$^-$) purified from cerebellum of P4 *Nestin-CFP–Actin-DsRed* mice differentiated into neurons, Bergmann glia and Purkinje neurons after the transplantation (data not shown). These data confirm that NEPs are lineage-committed neuronal progenitors.

In the studies above we focused on the differentiation potential of NEPs after isolation. To determine the fate of NEPs *in situ*, we lineage-traced these cells by using a *Nestin-CreER^{T2}* mouse, in which expression of a tamoxifen-regulatable Cre recombinase is controlled by the nestin enhancer[23]. We crossed *Nestin-CreER^{T2}* mice to *Gt(ROSA)26Sor* reporter (*R26R*) mice expressing *GFP* preceded by a *loxP*-flanked stop sequence[24]. After tamoxifen treatment at P4, *Nestin-CreER^{T2}–R26R-GFP* mice were killed at P21 to locate the GFP$^+$ cells in their cerebella by immunohistochemistry. 5–7% of the cells in the cerebellar internal granule layer (IGL)were GFP$^+$ (**Fig. 2j**). All of the GFP$^+$ cells in the IGL expressed Zic1 (**Fig. 2k**). We found no Calbindin$^+$ Purkinje neurons (**Fig. 2l**) or Parvalbumin$^+$ interneurons (**Fig. 2n**) among GFP$^+$ cells. GFP$^+$ cells in the molecular layer were glial cells that expressed S100β (**Fig. 2m**), presumably originating from Bergman glial cells expressing Nestin at P4. Some GFP$^+$ fibers remained on the surface of the *Nestin-CreER^{T2}–R26R-GFP* cerebellum at P21. These fibers did not have cell nuclei and were S100β$^+$ (**Supplementary Fig. 5**), suggesting that they represent end-feet of the Bergmann glial cells mentioned above. These data suggest that in addition to GNPs, NEPs also contribute to the genesis of granule neurons during cerebellar development.

NEPs and GNPs represent distinct lineages

It is generally believed that cerebellar granule neurons originate predominately from Math1$^+$ GNPs in the EGL[25]. Above we demonstrated that NEPs also generate granule neurons. We therefore examined the possible lineage relationships between NEPs and GNPs. For this purpose, we crossed *Math1-Cre–R26R-GFP* mice, which have previously been used to lineage-trace conventional GNPs[7,25], with *Nestin-CFP* animals. We microdissected cerebellar EGLs from these animals at P4 and dissociated them for FACS analysis. 58% of cells in the EGL were GFP$^+$, and ~4% of EGL cells at P4 were CFP$^+$ (**Fig. 3a**). We detected no GFP$^+$CFP$^+$ cell

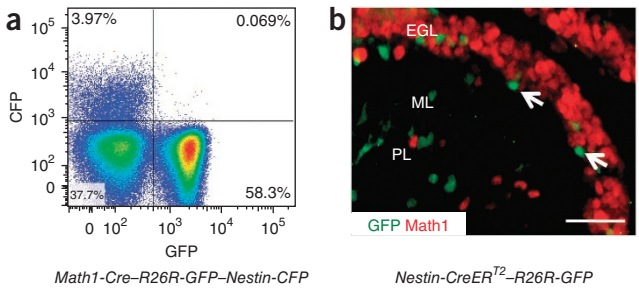

Figure 3 Lineage independence of NEPs and GNPs. (**a**) Flow cytometry analysis of cells dissected from the EGL of P4 *Math1-Cre–R26R-GFP–Nestin-CFP* mice for GFP and CFP expression. Numbers in quadrants indicate the proportion of cells in each section. (**b**) *Nestin-CreER^{T2}–R26R-GFP* mice were treated with tamoxifen at P4 and analyzed at P8. Cerebella were sectioned and stained for GFP and Math1. GFP$^+$ cells are marked with arrows. Scale bar, 200 μm.

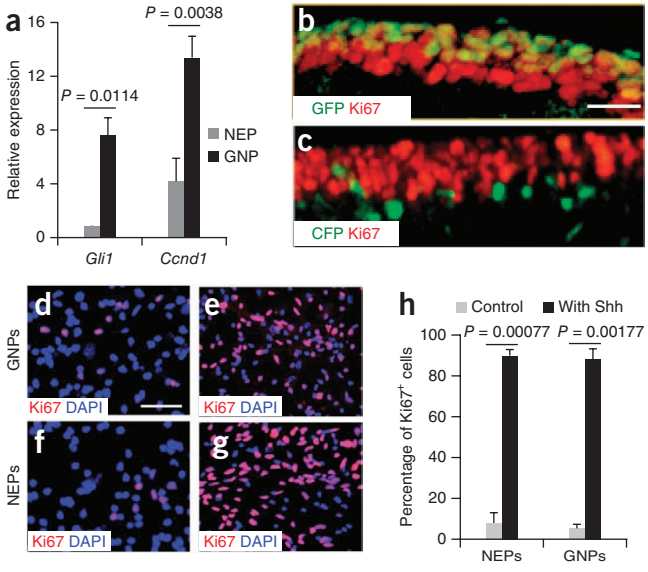

Figure 4 Shh-induced proliferation among NEPs. (**a**) Quantitative PCR analysis of *Gli1* and *Ccnd1* expression in NEPs and GNPs from cerebellum of P4 *Math1-GFP–Nestin-CFP* mice. Expression of both genes was normalized to that of actin. (**b**,**c**) Cerebellar sections from P4 *Math1-GFP* (**b**) or *Nestin-CFP* (**c**) mice immunostained for GFP or CFP and Ki67. Scale bar, 100 μm. (**d**–**g**) Micrographs of purified GNPs (**d**,**e**) and NEPs (**f**,**g**) cultured in the absence (**d**,**f**) and presence (**e**,**g**) of Shh, and then immunostained for Ki67 and counterstained with DAPI. Scale bar, 200 μm. (**h**) Percentage of Ki67$^+$ cells in cultured NEPs and GNPs with and without (Control) Shh treatment. Error bars (**a**,**h**), s.e.m. ($n = 3$). *P* values were calculated using two-tailed Student's *t* test.

population among EGL cells at P4 (**Fig. 3a**) or at later stages examined (P8–P15; data not shown). These results suggest that Math1$^+$ GNPs do not give rise to NEPs during cerebellar development.

To determine whether NEPs can give rise to GNPs, we crossed *Nestin-CreER^{T2}* mice to *R26R-GFP* mice to lineage-trace NEPs in the postnatal cerebellum. We treated *Nestin-CreER^{T2}–R26R-GFP* animals with tamoxifen at P4 and collected cerebella at P8 for immunostaining with antibodies to Math1 and GFP. Math1$^+$ GNPs were preferentially located in the outer part of cerebellar EGL (**Fig. 3b**). No Math1$^+$ GNPs expressed GFP at P8 or at later developmental stages (P10–P21, data not shown), suggesting that GNPs do not derive from NEPs in the developing cerebellum. The above data indicate that NEPs and GNPs are two independent cell lineages.

NEPs can proliferate in response to Sonic hedgehog

Shh protein, secreted by Purkinje neurons, is the major mitogen for GNPs in the EGL[26]. As NEPs residing in the inner EGL are closer to the source of Shh than GNPs are, they might be expected to show increased Shh signaling. To test this, we used quantitative PCR to measure expression of Shh pathway target genes (*Ccnd1*and *Gli1*) in NEPs and GNPs purified from *Math1-GFP–Nestin-CFP* cerebellum at P4. As expected, we detected very high levels of *Ccnd1* and *Gli1* in GNPs (**Fig. 4a**), consistent with the fact that Shh signaling occurrs in these cells. Expression of *Ccnd1* and *Gli1* was markedly lower in NEPs than in GNPs, suggesting that the Shh pathway was less active in NEPs. We then examined the proliferation of NEPs in the EGL by immunostaining cerebella from P4 *Nestin-CFP* and *Math1-GFP* mice with Ki67 antibodies. The majority of Math1$^+$ GNPs in the EGL were Ki67$^+$ (**Fig. 4b**), indicating that they are highly proliferative. In contrast, the majority of NEPs were Ki67$^-$ at P4 (**Fig. 4c**) and at all other stages examined (P0–P15, data not shown), suggesting that in contrast to GNPs, NEPs in the EGL are quiescent. Thus, despite being located proximal to the source of Shh (Purkinje neurons), NEPs do not appear to exhibit an active Shh signal pathway *in vivo*.

To test whether NEPs can respond to Shh, we purified GNPs and NEPs from cerebellum of P4 *Nestin-CFP–Math1-GFP* mice, treated them with recombinant Shh protein *in vitro* and examined their proliferation by immunostaining for Ki67. In the absence of Shh, the majority of both GNPs and NEPs stop dividing and become Ki67$^-$ after 48 h in culture (**Fig. 4d**,**f**), indicating that both cell populations are, or become, quiescent *in vitro* without Shh treatment. Consistent with previous studies[26,27], Shh dramatically increased the proliferation of GNPs (**Fig. 4e**,**h**), and to our surprise, proliferation of NEPs was also significantly ($P = 0.00077$; Student's *t* test) increased in the presence of Shh (**Fig. 4g**,**h**). These data suggest that NEPs have the capacity to respond to Shh *in vitro*, although they remain quiescent *in vivo*.

DNA repair–associated genes are downregulated in NEPs

The studies described above indicate that NEPs can give rise to granule neurons but are distinct from conventional GNPs. To determine the molecular basis for the difference between NEPs and GNPs,

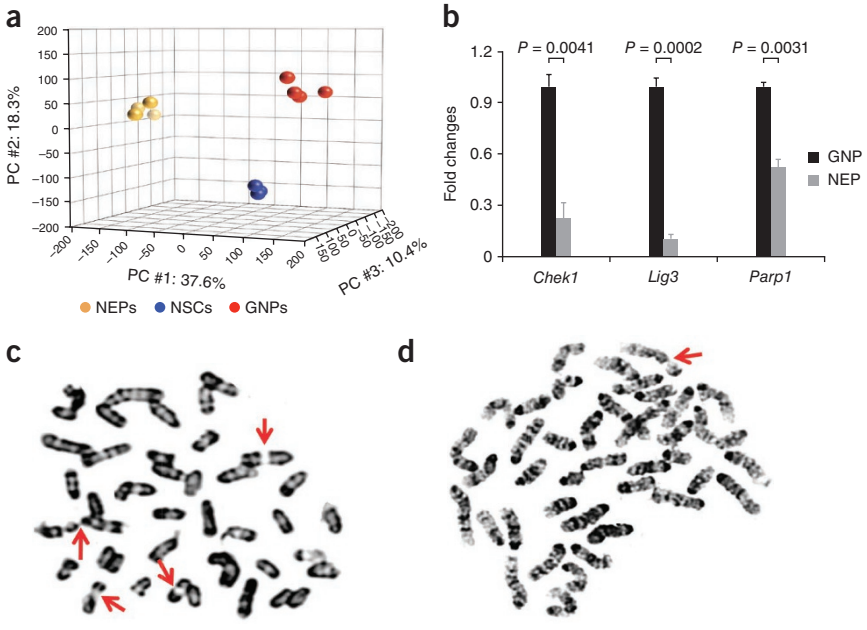

Figure 5 Deficiency in DNA repair of NEPs. (**a**) Principal component (PC) analysis. Each sample is represented by a spot whose position in the grid reflects its overall expression profile. The distance between spots is proportional to the difference in gene expression. Cumulative eigenvalue of the three principal components is 66.3%. (**b**) Quantitative PCR analysis of expression of indicated DNA-repair genes between NEPs and GNPs. Expression of all genes in NEPs is normalized to their relative expression in GNPs. Error bars, s.e.m. ($n = 3$). *P* values were calculated using two-tailed Student's *t* test. (**c**,**d**) Representative images of metaphase spreads from *Ptch1*-deficient NEPs (**c**) and GNPs (**d**). Arrows mark chromosomal breaks.

we performed gene expression analysis. RNA from NEPs, GNPs and NSCs purified from cerebellum of P4 *Nestin-CFP–Math1-GFP* mice was subjected to microarray analysis using Affymetrix mouse 430 2.0 chips. We then performed principal component analysis (PCA), a statistical method that facilitates global comparison of gene expression among multiple samples. NEPs, GNPs and NSCs were well separated from one another (**Fig. 5a**), confirming that NEPs are a unique progenitor population in the developing cerebellum.

To gain insight into properties that distinguish NEPs and GNPs, we examined the genes differentially expressed between these two cell populations. Among the 45,101 probe sets on the arrays, 4,902 (10.87%) showed significant differences in expression (increased or decreased by ≥2-fold, false discovery rate < 0.01 by paired *t* test). Among those, expression for 2,755 was higher in NEPs, and that for 2,147 was lower. Gene enrichment analysis using NexusExp3 software identified four major categories of genes that were differentially expressed between NEPs and GNPs (**Table 1**). Consistent with our observation that NEPs are normally quiescent *in vivo*, expression of genes associated with cell proliferation and cell cycle was markedly decreased in NEPs compared with GNPs. Cell adhesion and migration genes were also upregulated in NEPs, in agreement with the known involvement of Nestin in cell migration[5]. Genes involved in neural cell fate commitment were upregulated in NEPs relative to GNPs, consistent with the neuronal lineage restriction of NEPs. Finally, of 179 genes associated with DNA damage and repair, 62 (34.64%) were differentially expressed between NEPs and GNPs ($P < 0.001$). All 62 genes were downregulated in NEPs compared with GNPs. We validated the reduced expression of several DNA repair–associated genes in NEPs (including *Chek1*, *Lig3* and *Parp1*) by quantitative PCR (**Fig. 5b**).

Table 1 Categories of genes differentially expressed in NEPs versus GNPs

Gene name	Gene symbol	Log ratio	Gene function
Cell cycle			
E2F transcription factor 1	*E2f1*	−2.2	Cell cycle control
Cyclin D1	*Ccnd1*	−2.0	Cell cycle G1-S transition
Cyclin G2	*Ccng2*	−1.7	Cell cycle control
Structural maintenance of chromosomes 2	*Smc2*	−1.7	Chromatid cohesion and chromosome condensation
Cell division cycle associated 5	*Cdca5*	−1.6	Cell cycle G1-S transition
Cyclin-dependent kinase 6	*Cdk6*	−1.2	G1 phase transition of cell cycle
DNA damage or repair			
Breast cancer 1	*Brca1*	−1.9	DNA damage response
Rad51 associated protein-1	*Rad51ap1*	−1.6	DNA recombination and repair
Brca1/Brca2-containing complex, subunit 3	*Brcc3*	−1.1	DNA damage and repair
Brca2 and Cdkn1a interacting protein	*Bccip*	−1.0	DNA damage and repair
Checkpoint kinase 1	*Chek1*	−0.9	DNA damage checkpoint and DNA repair
DNA ligase 3	*Lig3*	−0.6	DNA recombination and repair
Poly (ADP-ribose) polymerase 1	*Parp1*	−0.5	DNA repair
Cell adhesion and migration			
Tenascin C	*Tnc*	8.2	Fibronectin binding
Procollagen, type 1, alpha 2	*Col1a2*	6.7	Extracellular matrix structural constituent
Vascular cell adhesion molecule 1	*Vcam1*	6.4	GPI anchor binding and protein binding
Neuropilin 1	*Nrp1*	5.0	Semaphorin receptor regulation
Developmentally downregulated 9	*Nedd9*	4.3	Cell adhesion and protein binding
Neural cell adhesion molecule 2	*Ncam2*	3.3	GPI anchor binding
Protocadherin 17	*Pcdh17*	2.6	Calcium ion binding
Neural fate commitment			
Pancreas specific transcription factor 1a	*Ptf1a*	7.8	Neural fate commitment
Neurogenin 2	*Neurog2*	6.3	Neural differentiation and lineage commitment
Neurogenin 1	*Neurog1*	5.0	Neural differentiation and lineage commitment
Notch gene homolog 1	*Notch1*	4.5	Notch1 signaling and fate commitment
SRY-box containing gene 6	*Sox6*	4.3	Neural lineage commitment
Sprouty homolog 2	*Spry2*	2.9	Cell fate commitment

The quiescent status of cells, particularly stem cells, has been suggested to be an essential protective mechanism that minimizes endogenous stress caused by cellular respiration and DNA replication[28]. To determine whether the decreased expression of DNA repair–associated genes in NEPs is due to their quiescent status, we induced the proliferation of NEPs and GNPs by exposing them to recombinant Shh. After 48 h, we harvested cells for quantitative PCR analysis. Expression of *Chek1*, *Lig3* and *Parp1* was significantly lower (two-tailed Student's *t* test; *Chek1*, $P = 0.00085$; *Lig3*, $P = 0.0171$; *Parp1*, $P = 0.0106$) in proliferating NEPs than GNPs (**Supplementary Fig. 6**). These data suggest that decreased expression of DNA repair–associated genes in NEPs is independent of their quiescent state. The above results indicate that NEPs have a distinct genetic profile characterized by decreased expression of DNA repair–associated transcripts.

Proliferative stress causes DNA instability in NEPs

The cellular DNA repair machinery is critical for maintaining the genomic integrity that is constantly challenged by endogenous and exogenous stimuli[29]. The decreased expression of DNA repair genes in NEPs raises the possibility that these cells may be more susceptible to DNA damage in response to genotoxic agents and stress. Because hyperproliferation can cause DNA-replication stress and genomic damage[30], we compared the genomic alterations in hyper-proliferating NEPs and GNPs. For this purpose, we crossed *Math1-GFP–Nestin-CFP* mice with *Ptch1*$^{C/C}$ mice, in which the *loxP*-flanked Patched1 (*Ptch1*) gene can be conditionally ablated in a Cre recombinase–dependent manner[31]. Ptch1 is an antagonist of the Shh signaling pathway, so *Ptch1* deletion causes aberrant activation of Shh signaling and hyperproliferation in both stem cells and progenitors in the nervous system[7,32,33]. We purified NEPs and GNPs from P4 *Math1-GFP–Nestin-CFP–Ptch1*$^{C/C}$ cerebella and deleted *Ptch1* in these cells by infection with a lentivirus encoding Cre recombinase. 24 h after infection, we pulse-labeled the cells with BrdU for an additional 12 h and then collected them for analysis of BrdU incorporation by immunocytochemistry. We observed extensive and comparable proliferation among GNPs and NEPs infected with lentivirus encoding Cre recombinase (**Supplementary Fig. 6c**)[7]. We then harvested these two cell populations to perform metaphase spreading to test for the presence of chromosomal aberrations, which is the major form of genomic instability in mammalian cells[34]. We found more chromosome alterations including chromosomal breaks, centromere separation and pulverization in NEPs (62.96%) compared with GNPs (20.0%), suggesting that NEPs exhibit greater genomic instability after *Ptch1* deletion (**Fig. 5c**,**d** and **Supplementary Fig. 6d**).

NEPs exhibit increased tumorigenic potential

It has been reported that genomic instability facilitates tumorigenesis in many cells, including neuronal progenitors[14,35]. We had previously

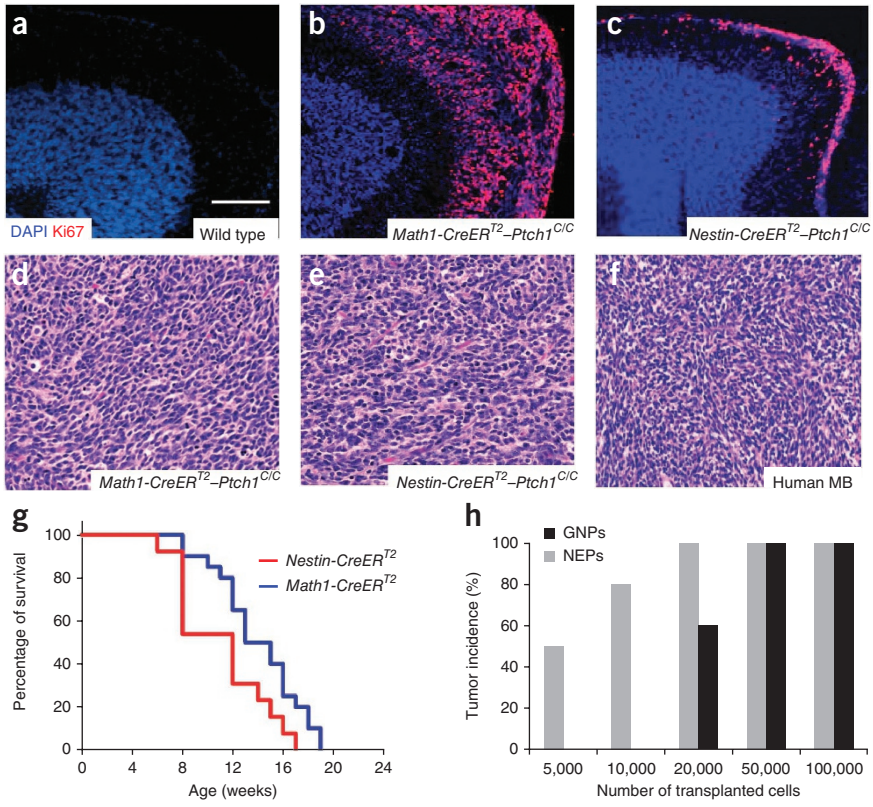

Figure 6 Increased tumorigenicity of NEPs after *Ptch1* deletion. (**a**–**c**) Cerebellar sections prepared from P21 wild type mice (**a**), *Math1-CreER^{T2}–Ptch1$^{C/C}$* mice (**b**) and *Nestin-CreER^{T2}–Ptch1$^{C/C}$* mice (**c**) at P21, immunostained for Ki67 (red) and counterstained with DAPI (blue). Note the ectopic lesions on the surface of the cerebellum after *Ptch1* deletion. (**d**–**f**) Hematoxylin and eosin staining of paraffin-embedded tumor sections prepared from *Math1-CreER^{T2}–Ptch1$^{C/C}$* mice (**d**), *Nestin-CreER^{T2}–Ptch1$^{C/C}$* mice (**e**) and human medulloblastoma (**f**). Scale bar, 200 µm. (**g**) Survival curve of *Math1-CreER^{T2}–Ptch1$^{C/C}$* mice and *Nestin-CreER^{T2}–Ptch1$^{C/C}$* mice after tamoxifen treatment at P4. Both NEPs and GNPs gave rise to tumors after *Ptch1* deletion with 100% penetrance. Mantel-Cox test, $P = 0.0283$, $n = 12$ for *Nestin-CreER^{T2}–Ptch1$^{C/C}$* mice, $n = 14$ for *Math1-CreER^{T2}–Ptch1$^{C/C}$* mice. (**h**) The tumor incidence in SCID animals after transplantation with indicated number of *Ptch1*-deficient GNPs and NEPs.

demonstrated that deletion of *Ptch1* in GNPs causes medulloblastoma formation in mice[7]. The fact that *Ptch1* deletion promotes proliferation and genomic instability in NEPs led us to postulate that NEPs may be more susceptible to oncogenic transformation after loss of *Ptch1*. To test this, we crossed *Ptch1$^{C/C}$* mice, with *Nestin-CreER^{T2}* mice. For comparison, we also deleted *Ptch1* in GNPs using *Math1-CreER^{T2}* mice[7,25]. We treated animals with tamoxifen at P4 and examined cerebella at P21, a time point at which wild-type GNPs have exited the cell cycle, differentiated and migrated inward from the surface of the cerebellum (**Fig. 6a**). As reported previously[7], we found large numbers of proliferating cells on the surface of the cerebellum in P21 *Math1-CreER^{T2}–Ptch1$^{C/C}$* animals (**Fig. 6b**). We detected far fewer ectopically proliferating cells in the *Nestin-CreER^{T2}–Ptch1$^{C/C}$* cerebellum at P21 (**Fig. 6c**), consistent with the relatively small number of NEPs in the cerebellum at the time of tamoxifen treatment (NEPs account for only 3–5% of EGL cells at P4). Notably, both *Nestin-CreER^{T2}–Ptch1$^{C–C}$* animals and *Math1-CreER^{T2}/Ptch1$^{C/C}$* animals eventually developed tumors. These tumors resemble human medulloblastoma in terms of histology (**Fig. 6d**–**f**). Moreover, tumor cells from *Nestin-CreER^{T2}–Ptch1$^{C/C}$* and *Math1-CreER^{T2}–Ptch1$^{C/C}$* mice exhibited very similar gene expression profiles based on principal component analysis (**Supplementary Fig. 7**). Thus, NEPs can also give rise to medulloblastoma after loss of *Ptch1*.Despite being far less abundant than GNPs, NEPs give rise to tumors with the same penetrance (100%) and latency as Math1$^+$ GNPs (**Fig. 6g**). These findings suggest that on a per-cell basis, NEPs may be more prone to give rise to tumors than GNPs.

To directly compare the tumorigenic potential of NEPs and GNPs, we performed limiting dilution transplantation assays. For this purpose, we generated *Nestin-CreER^{T2}–Nestin-CFP–Ptch1$^{C/C}$* mice and *Math1-CreER^{T2}–Math1-GFP–Ptch1$^{C/C}$* mice. After treatment of these animals with tamoxifen at P4, we microdissected EGLs at P8. We isolated NEPs and GNPs with deleted *Ptch1* from the dissociated EGLs by FACS-sorting CFP$^+$ and GFP$^+$ cells, respectively. We confirmed comparable efficiency of *Ptch1* deletion in the two purified cell populations by quantitative PCR as previously described[7] (**Supplementary Fig. 8a**–**c**). Transplantation of more than 50,000 NEPs or GNPs resulted in tumor formation in 100% of recipients (**Fig. 6h** and **Supplementary Fig. 8d**). Transplantation of 20,000 GNPs resulted in tumors in 60% of recipients, whereas the same number of NEPs still generated tumors in 100% of recipients. Transplantation of fewer than 20,000 GNPs did not cause tumor formation, but as few as 5,000 NEPs generated medulloblastoma in 50% of recipients. These data confirm that NEPs have increased tumorigenic potential compared to GNPs.

DISCUSSION

Nestin is widely considered a marker for NSCs in various regions of the nervous system, but is commonly lost as NSCs differentiate into lineage-restricted neuronal and glial progenitors[2]. Here we describe a previously unidentified population of Nestin-expressing cells in the EGL of the developing cerebellum. These cells did not exhibit stem cell properties such as neurosphere-forming capacity and multipotency, and exclusively generated granule neurons. These data suggest that some neuronal progenitors retain Nestin expression during differentiation.

Although they are committed to the granule neuron lineage, NEPs are apparently distinct from conventional GNPs in that NEPs account for only 3–5% of the cells that can be isolated from the EGL, whereas GNPs account for over 90% of EGL cells; NEPs do not express Math1, a transcription factor previously thought to be essential for specification of GNPs[17]; NEPs reside in the deep part of the EGL, whereas GNPs are found in the superficial EGL; GNPs proliferate extensively in the EGL, whereas NEPs migrate and differentiate without initial proliferating; and the expression profile of NEPs is distinct from that of GNPs. Together, these data suggest that NEPs represent a unique population of granule neuron progenitors. Previous studies have suggested that cerebellar granule neurons predominately originate from Math1-expressing GNPs[25]. However, our studies demonstrate that NEPs also contribute to the genesis of granule neurons. We have not observed any obvious phenotypic or morphological differences

between granule neurons originating from NEPs and those arising from conventional GNPs, but additional studies will be necessary to determine whether there are functional distinctions between these two populations.

The ability of NEPs to give rise to granule neurons despite their lack of Math1 expression is somewhat surprising. Math1 is highly expressed in GNPs located in the anterior rhombic lip as well as the outer part of the EGL[17]. The fact that Math1-deficient animals lack an EGL has often been interpreted to mean that Math1 is required for GNP regeneration. Our observation that NEPs can produce granule neurons suggests that Math1 is not absolutely required for specification or maintenance of granule neuron identity. Although our studies have revealed that NEPs and GNPs are mutually exclusive during cerebellar development, it is possible that NEPs and GNPs have a common cellular origin: NSCs in the ventricular zone[15]. It has been demonstrated that GNPs originate from progenitors in the rhombic lip[10]. However, we detected no Nestin-expressing cells in the rhombic lip at embryonic stages (**Supplementary Fig. 1**), and NEPs are always found in the deep part of the EGL, implying that NEPs are not rhombic lip-derived progenitors. Other possible sources of NEPs include NSCs in the embryonic ventricular zone or postnatal white matter[6], or astroglial cells in the EGL[36].

A recent study identified a new population of GFAP$^+$ cells in the EGL by using transgenic mice expressing *DsRed* driven by the human *GFAP* promoter[36]. DsRed$^+$ cells expressed Nestin, reside in the deep part of EGL and to give rise to granule neurons. However, 60% of GFAP$^+$ cells were Musashi1$^+$, and almost half of GFAP$^+$ cells were Ki67$^+$. Based on these immunostaining data, the authors concluded that GFAP$^+$ cells in the EGL represent NSCs. In contrast, the NEPs we identified in our study were quiescent and did not exhibit multipotency or the ability to form neurospheres. Given these differences, we believe that NEPs and GFAP$^+$ cells in the EGL are distinct populations.

Shh is a potent mitogen for GNPs in the developing cerebellum. Despite residing in a Shh-enriched environment, NEPs do not express Shh target genes and do not proliferate *in vivo*. However, NEPs markedly increase their proliferation in response to Shh *in vitro*. These data suggest that NEPs have the capacity to respond to Shh signaling. The failure of NEPs to respond to Shh *in vivo* may be due to factors in the inner EGL that override the mitogenic effects of Shh. For example, pituitary adenylate cyclase activating polypeptide[37], bone morphogenetic proteins[38], FGF-2 (ref. 39) and the extracellular matrix molecule vitronectin[40] have all been shown to inhibit Shh-induced proliferation of GNPs. Additional experiments will be necessary to delineate the contribution of these signals to the quiescent state of NEPs *in vivo*.

It has been reported that GNPs can give rise to medulloblastoma after aberrant activation of Shh signaling[7,41]. In this study, we demonstrated that NEPs also have the capacity to initiate medulloblastoma formation after deletion of *Ptch1*. We did not find any obvious differences between tumors arising from GNPs and those derived from NEPs based on thymidine incorporation, cell-cycle analysis and gene expression profiling. These studies suggest that both NEPs and GNPs can represent cells of origin for Shh-associated medulloblastoma. Notably, expression of Shh in Nestin$^+$ cells using the *RCAS-TVA* system also results in medulloblastoma[12]. Although previous studies have suggested that these tumors arise from GNPs, our studies raise the possibility that they may actually originate from NEPs.

Cell proliferation involves many processes that need to be tightly coordinated to ensure the preservation of genome integrity and to promote faithful genome propagation. Efficient and error-free DNA replication is critical for faithful replication of chromosomes before their segregation. Coordination of DNA replication with DNA-damage repair ensures genome integrity during cell division, thus preventing tumorigenic mutations. It has been reported that disruption of a DNA repair pathway has the potential to expedite tumorigenesis by resulting in a cell that is hypermutable[42,43]. In this study, we demonstrated that NEPs exhibit more chromosomal aberrations after *Ptch1* deletion than GNPs. In our previous studies, we have demonstrated that loss of *Ptch1* alone is not sufficient to initiate tumor formation and that additional epigenetic or genetic changes ('second hits') are required to fully transform GNPs[7,44]. Comparable levels of proliferation of NEPs and GNPs after deletion of *Ptch1* (**Fig. 5c**) indicate that the differential tumorigenic potential of these two cell populations is not solely due to deletion of *Ptch1*. Deficiency in DNA repair may give NEPs advantages in terms of accumulating the oncogenic mutations necessary for tumor initiation, and this may result in the increased tumorigenicity of NEPs after deletion of *Ptch1*.

The fact that NEPs exhibit increased genomic instability and increased tumorigenic potential is consistent with previous studies showing that genomic instability facilitates formation of medulloblastoma in neuronal progenitors. Ionizing radiation dramatically increases tumor incidence and accelerates medulloblastoma formation in *Ptch1*$^{+/-}$ mice, suggesting that DNA damage results in predisposition to medulloblastoma tumorigenesis[45,46]. Moreover, inactivation of DNA repair–associated genes, including *Lig4*, *Xrcc4* and *Brca2* in cerebellar neuronal progenitors (using a *Nestin-Cre* transgene), has been reported to cause formation of medulloblastoma in a p53-deficient background[14,35,47]. A very recent study has also shown that overexpression of Yes-associated protein (YAP) impairs DNA repair and increases medulloblastoma tumorigenesis in cerebellar neuronal progenitors[48]. Our observation that NEPs are already deficient in DNA repair suggests that these cells may be particularly prone to transformation and may represent cells of origin in some of the above tumor models.

It is common to think of oncogenic transformation as resulting from a series of mutations that endow a cell with increased genomic instability, unlimited proliferative capacity, decreased ability to undergo apoptosis and altered ability to interact with the microenvironment. However, our studies suggest that these properties may not necessarily be the result of somatic mutations, but instead, may represent intrinsic characteristics of cells at certain stages of development. Indeed, transgenic expression of the same oncogene or conditional deletion of the same tumor suppressor gene in different tissues under the control of tissue-specific promoters frequently results in remarkable variations in tumor-initiating capability, phenotype, latency and penetrance[49]. These examples highlight the critical role of the cellular context in determining whether and when tumorigenesis will take place in response to particular oncogenic stimuli. Identification of 'tumor-prone' cell populations may provide critical insight into mechanisms of transformation and yield new approaches to targeting cancer.

METHODS

Methods and any associated references are available in the online version of the paper.

Accession codes. Gene Expression Omnibus: GSE50824.

Note: Any Supplementary Information and Source Data files are available in the online version of the paper.

ACKNOWLEDGMENTS

We thank J. Oesterling for flow cytometric analysis; Z. Liu, J. Pei and J. Testa for cytogenetic analysis; A. Efimov for microscopy analysis; Q. Cai for histological analysis; R. Segal (Dana Farber Cancer Institute) for Zic1 antibody; and D. Wiest, F. Roegiers and T. Yen for helpful discussions. This research was supported by

the W.W. Smith Charitable Trust (Z.Y.), a generous gift from Cathie and Pete Getchell (Z.Y.), a US National Institutes of Health Postdoctoral training grant (5T32CA009035-37, L.W.Y.), grants from the US National Cancer institute (R01-CA178380, Z.Y.; R01-CA122759, R.J.W.-R.), pilot funding from the US National Institutes of Health (U19-AI067798, R.J.W.-R.) and the California Institute for Regenerative Medicine (LA1-01747, R.J.W.-R.).

AUTHOR CONTRIBUTIONS

Z.Y. and R.J.W.-R. conceived the project. P.L., F.D., L.W.Y., T.L., R.E.M. and R.T. performed the experiments. Z.Y., P.L., J.W., A.B. and R.J.W.-R. analyzed the data. G.E. provided reagents. Z.Y. prepared the manuscript.

COMPETING FINANCIAL INTERESTS

The authors declare no competing financial interests.

1. Lendahl, U., Zimmerman, L.B. & McKay, R.D. CNS stem cells express a new class of intermediate filament protein. *Cell* **60**, 585–595 (1990).
2. Morshead, C.M. *et al.* Neural stem cells in the adult mammalian forebrain: a relatively quiescent subpopulation of subependymal cells. *Neuron* **13**, 1071–1082 (1994).
3. Shi, H. *et al.* Nestin expression defines both glial and neuronal progenitors in postnatal sympathetic ganglia. *J. Comp. Neurol.* **508**, 867–878 (2008).
4. Vukojevic, K., Petrovic, D. & Saraga-Babic, M. Nestin expression in glial and neuronal progenitors of the developing human spinal ganglia. *Gene Expr. Patterns* **10**, 144–151 (2010).
5. Hyder, C.L., Isoniemi, K.O., Torvaldson, E.S. & Eriksson, J.E. Insights into intermediate filament regulation from development to ageing. *J. Cell Sci.* **124**, 1363–1372 (2011).
6. Lee, A. *et al.* Isolation of neural stem cells from the postnatal cerebellum. *Nat. Neurosci.* **8**, 723–729 (2005).
7. Yang, Z.J. *et al.* Medulloblastoma can be initiated by deletion of Patched in lineage-restricted progenitors or stem cells. *Cancer Cell* **14**, 135–145 (2008).
8. Sutter, R. *et al.* Cerebellar stem cells act as medulloblastoma-initiating cells in a mouse model and a neural stem cell signature characterizes a subset of human medulloblastomas. *Oncogene* **29**, 1845–1856 (2010).
9. Sotelo, C., Alvarado-Mallart, R.M., Frain, M. & Vernet, M. Molecular plasticity of adult Bergmann fibers is associated with radial migration of grafted Purkinje cells. *J. Neurosci.* **14**, 124–133 (1994).
10. Alder, J., Cho, N.K. & Hatten, M.E. Embryonic precursor cells from the rhombic lip are specified to a cerebellar granule neuron identity. *Neuron* **17**, 389–399 (1996).
11. Rao, G., Pedone, C.A., Coffin, C.M., Holland, E.C. & Fults, D.W. c-Myc enhances sonic hedgehog-induced medulloblastoma formation from nestin-expressing neural progenitors in mice. *Neoplasia* **5**, 198–204 (2003).
12. Rao, G. *et al.* Sonic hedgehog and insulin-like growth factor signaling synergize to induce medulloblastoma formation from nestin-expressing neural progenitors in mice. *Oncogene* **23**, 6156–6162 (2004).
13. Tanori, M. *et al.* Developmental and oncogenic effects of insulin-like growth factor-I in Ptc1$^{+/-}$ mouse cerebellum. *Mol. Cancer* **9**, 53 (2010).
14. Frappart, P.O., Lee, Y., Lamont, J. & McKinnon, P.J. BRCA2 is required for neurogenesis and suppression of medulloblastoma. *EMBO J.* **26**, 2732–2742 (2007).
15. Mills, J. *et al.* Critical role of integrin-linked kinase in granule cell precursor proliferation and cerebellar development. *J. Neurosci.* **26**, 830–840 (2006).
16. Encinas, J.M., Vaahtokari, A. & Enikolopov, G. Fluoxetine targets early progenitor cells in the adult brain. *Proc. Natl. Acad. Sci. USA* **103**, 8233–8238 (2006).
17. Ben-Arie, N. *et al.* Math1 is essential for genesis of cerebellar granule neurons. *Nature* **390**, 169–172 (1997).
18. Lumpkin, E.A. *et al.* Math1-driven GFP expression in the developing nervous system of transgenic mice. *Gene Expr. Patterns* **3**, 389–395 (2003).
19. Uchida, N. *et al.* Direct isolation of human central nervous system stem cells. *Proc. Natl. Acad. Sci. USA* **97**, 14720–14725 (2000).
20. Reynolds, B.A. & Weiss, S. Generation of neurons and astrocytes from isolated cells of the adult mammalian central nervous system. *Science* **255**, 1707–1710 (1992).
21. Vintersten, K. *et al.* Mouse in red: red fluorescent protein expression in mouse ES cells, embryos, and adult animals. *Genesis* **40**, 241–246 (2004).
22. Aruga, J. *et al.* A novel zinc finger protein, zic, is involved in neurogenesis, especially in the cell lineage of cerebellar granule cells. *J. Neurochem.* **63**, 1880–1890 (1994).
23. Balordi, F. & Fishell, G. Mosaic removal of hedgehog signaling in the adult SVZ reveals that the residual wild-type stem cells have a limited capacity for self-renewal. *J. Neurosci.* **27**, 14248–14259 (2007).
24. Mao, X., Fujiwara, Y., Chapdelaine, A., Yang, H. & Orkin, S.H. Activation of EGFP expression by Cre-mediated excision in a new ROSA26 reporter mouse strain. *Blood* **97**, 324–326 (2001).
25. Machold, R. & Fishell, G. Math1 is expressed in temporally discrete pools of cerebellar rhombic-lip neural progenitors. *Neuron* **48**, 17–24 (2005).
26. Wechsler-Reya, R.J. & Scott, M.P. Control of neuronal precursor proliferation in the cerebellum by Sonic Hedgehog. *Neuron* **22**, 103–114 (1999).
27. Kenney, A.M., Cole, M.D. & Rowitch, D.H. Nmyc upregulation by sonic hedgehog signaling promotes proliferation in developing cerebellar granule neuron precursors. *Development* **130**, 15–28 (2003).
28. Orford, K.W. & Scadden, D.T. Deconstructing stem cell self-renewal: genetic insights into cell-cycle regulation. *Nat. Rev. Genet.* **9**, 115–128 (2008).
29. Lombard, D.B. *et al.* DNA repair, genome stability, and aging. *Cell* **120**, 497–512 (2005).
30. Burhans, W.C. & Weinberger, M. DNA replication stress, genome instability and aging. *Nucleic Acids Res.* **35**, 7545–7556 (2007).
31. Ellis, T. *et al.* Patched 1 conditional null allele in mice. *Genesis* **36**, 158–161 (2003).
32. Ahn, S. & Joyner, A.L. *In vivo* analysis of quiescent adult neural stem cells responding to Sonic hedgehog. *Nature* **437**, 894–897 (2005).
33. Balordi, F. & Fishell, G. Hedgehog signaling in the subventricular zone is required for both the maintenance of stem cells and the migration of newborn neurons. *J. Neurosci.* **27**, 5936–5947 (2007).
34. Aguilera, A. & Gomez-Gonzalez, B. Genome instability: a mechanistic view of its causes and consequences. *Nat. Rev. Genet.* **9**, 204–217 (2008).
35. Frappart, P.O. *et al.* Recurrent genomic alterations characterize medulloblastoma arising from DNA double-strand break repair deficiency. *Proc. Natl. Acad. Sci. USA* **106**, 1880–1885 (2009).
36. Silbereis, J. *et al.* Astroglial cells in the external granular layer are precursors of cerebellar granule neurons in neonates. *Mol. Cell. Neurosci.* **44**, 362–373 (2010).
37. Nicot, A., Lelievre, V., Tam, J., Waschek, J.A. & DiCicco-Bloom, E. Pituitary adenylate cyclase-activating polypeptide and sonic hedgehog interact to control cerebellar granule precursor cell proliferation. *J. Neurosci.* **22**, 9244–9254 (2002).
38. Rios, I., Alvarez-Rodriguez, R., Marti, E. & Pons, S. Bmp2 antagonizes sonic hedgehog-mediated proliferation of cerebellar granule neurones through Smad5 signalling. *Development* **131**, 3159–3168 (2004).
39. Fogarty, M.P., Kessler, J.D. & Wechsler-Reya, R.J. Morphing into cancer: the role of developmental signaling pathways in brain tumor formation. *J. Neurobiol.* **64**, 458–475 (2005).
40. Pons, S., Trejo, J.L., Martinez-Morales, J.R. & Marti, E. Vitronectin regulates Sonic hedgehog activity during cerebellum development through CREB phosphorylation. *Development* **128**, 1481–1492 (2001).
41. Schuller, U. *et al.* Acquisition of granule neuron precursor identity is a critical determinant of progenitor cell competence to form Shh-induced medulloblastoma. *Cancer Cell* **14**, 123–134 (2008).
42. Kaye, J.A. *et al.* DNA breaks promote genomic instability by impeding proper chromosome segregation. *Curr. Biol.* **14**, 2096–2106 (2004).
43. Jasin, M. Chromosome breaks and genomic instability. *Cancer Invest.* **18**, 78–86 (2000).
44. Oliver, T.G. *et al.* Loss of patched and disruption of granule cell development in a pre-neoplastic stage of medulloblastoma. *Development* **132**, 2425–2439 (2005).
45. Pazzaglia, S. *et al.* High incidence of medulloblastoma following X-ray-irradiation of newborn Ptc1 heterozygous mice. *Oncogene* **21**, 7580–7584 (2002).
46. Pazzaglia, S. *et al.* The genetic control of chemically and radiation-induced skin tumorigenesis: a study with carcinogenesis-susceptible and carcinogenesis-resistant mice. *Radiat. Res.* **158**, 78–83 (2002).
47. Lee, Y. & McKinnon, P.J. DNA ligase IV suppresses medulloblastoma formation. *Cancer Res.* **62**, 6395–6399 (2002).
48. Fernandez, L.A. *et al.* Oncogenic YAP promotes radioresistance and genomic instability in medulloblastoma through IGF2-mediated Akt activation. *Oncogene* **31**, 1923–1937 (2012).
49. Beer, S. *et al.* Developmental context determines latency of MYC-induced tumorigenesis. *PLoS Biol.* **2**, e332 (2004).

ONLINE METHODS

Animals. *Ptch1*$^{C/C}$ mice, *Nestin-CFP* mice and *Nestin-CreER*^{T2} mice have been described previously[23,31]. *Math1-Cre* mice, *Math1-CreER*^{T2} mice, *Math1-GFP* mice, *Actin-DsRed* mice and *R26R-GFP* reporter mice were purchased from the Jackson Laboratory. SCID mice (C.B-17 SCID) were bred in the Fox Chase Cancer Center Laboratory Animal Facility. All animals were maintained in the Laboratory Animal Facility at Fox Chase Cancer Center, and all experiments were performed in accordance with procedures approved by the Fox Chase Cancer Center Animal Care and Use Committee. In this study, we used mice of either sex at various ages, which are mentioned in the text and figure legends.

Cerebellum microdissection, cell isolation and cell culture. Cerebella were harvested from *Nestin-CFP–Math1-GFP* animals at P4. 300-μm slices were prepared using a VT1000S vibratome (Leica). Under a fluorescence microscope, EGL or white matter were carefully removed from the rest of the cerebellum using fine forceps. Dissected EGL or white matter were then digested in a solution containing 10 units/ml papain (Worthington) and 250 U/ml DNase then triturated to obtain a single-cell suspension. GNPs (GFP$^+$) and NEPs (CFP$^+$) were then purified using a FACSvantage SEM (BD Bioscience). For isolation of NSCs, the cell suspension dissociated from *Nestin-CFP–Math1-GFP* cerebellum was stained for 1 h with PE-conjugated Prominin1 antibody and with antibodies specific for lineage markers (PSA-NCAM, O4 and TAPA-1; sources, identifiers and dilutions used for all antibodies are listed in **Supplementary Table 1**). After staining with FITC-conjugated secondary antibodies, NSCs were FACs sorted for PE-positive and FITC-negative cells[6].

NEPs and GNPs were suspended in NB-B27 (Neurobasal with 1 mM sodium pyruvate, 2 mM L-glutamine, penicillin-streptomycin and B27 supplement; all from Invitrogen) and plated on poly(D-lysine) (PDL)-coated coverslips (BD Biosciences). For the neurosphere-forming assay, cells were plated at 2×10^5 cells/ml in NSC proliferation medium (NeuroCult basal medium with proliferation supplemental; Stem Cell Technologies) plus 10 ng/ml basic fibroblast growth factor and 20 ng/ml epidermal growth factor (Pepro Tech). Neurospheres were counted or harvested for immunostaining after 7 d in culture. To confirm the self-renewal capacity, neurospheres were mechanically dissociated and replated in fresh proliferation medium at 2×10^3 cells/ml. For differentiation assays, cells were plated on PDL-coated coverslips in NSC differentiation medium (NeuroCult basal medium with differentiation supplement; Invitrogen).

Immunochemical staining and histological analysis. For tissue staining, cerebella from PFA-perfused animals were fixed overnight in 4% PFA, cryoprotected in 30% sucrose, frozen in Tissue Tek-OCT (Sakura Finetek) and cut into 10–12 μm sagittal sections. For cell staining, GNPs cultured on PDL were fixed with 4% PFA for 15 min. Immunofluorescence staining of sections and cells was carried out according to standard methods. Briefly, sections or cells were blocked and permeabilized for 2 h with PBS containing 0.1% Triton X-100 and 1% normal goat serum, stained with primary antibodies overnight at 4 °C, and incubated with secondary antibodies for 2 h at room temperature. Sections or cells were counterstained with DAPI and mounted with Fluoromount-G (Southern Biotech) before being visualized using a Nikon TE200 microscope. Antibodies used in this study are listed in **Supplementary Table 1**. To compare the histological properties between human and mouse medulloblastoma, hematoxylin and eosin stain was performed according to a standard procedure. Human medulloblastoma slides were purchased from US Biomax, Inc.

Tamoxifen treatment and intracranial transplantation. Tamoxifen (Sigma) was prepared as a 20 mg/ml stock solution in corn oil (Sigma) and was administered by oral gavage using a 24G gavaging needle (Fine Science Tools). Animals at P4 were given tamoxifen at a dosage of 0.6 mg/30 ml.

For the intracranial transplantations, SCID mice were anesthetized using 100 mg/kg ketamine (Fort Dodge Animal Health) plus 9 mg/kg xylazine (Ben Venue Laboratories) and positioned in a stereotaxic frame with a mouse adaptor (David Kopf Instruments). An incision was made in the midline of the scalp over the cerebellum, and a small hole was made in the skull (1 mm lateral to midline) using a beveled 18G needle. A 24G Hamilton syringe loaded with cells was mounted on a micromanipulator and introduced through the hole at a 30° angle to the surface of the cerebellum at a depth of 1 mm. Freshly sorted (uncultured) cells were injected over the course of 2 min, and the needle was left in place for another 2 min to avoid reflux. After removing the mouse from the frame, 1–2 drops of 0.25% (2.5 mg/ml) bupivicaine (Hospira) were applied along the incision for postoperative analgesia and the skin was closed with 6.0 fast-absorbing plain gut sutures using a 3/8 PC-1 cutting needle (Ethicon).

Microarray analysis. RNAs isolated from NEPs, GNPs and NSCs were labeled and hybridized to Affymetrix Mouse Genome 430 2.0 arrays. Microarray data were preprocessed using robust multichip analysis (RMA). Principal component analysis (PCA) was performed on samples based on normalized expression of all genes using Partek Genomics Suite 6.3 software. Gene ontology analysis was carried out to examine the biological functions of the differentially expressed genes between NEPs and GNPs using NexusExp3 software.

Quantitative PCR. RNA was isolated using the RNAqueous kit (Ambion) and treated with DNA-free DNase (Ambion). cDNA was synthesized using oligo(dT) and Superscript II reverse transcriptase (Invitrogen). Quantitative PCR reactions were performed in triplicate using iQ SYBR Green Supermix (Bio-Rad) and the Bio-Rad iQ5 Multicolor Real-Time PCR Detection System. Gene expression was normalized to actin and expression of each gene was compared between NEPs and GNPs. Primer sequences are available upon request.

Metaphase spread. Metaphase preparations were carried out by the Molecular Cytogenetics core facility at Fox Chase Cancer Center according to standard procedures.

Statistics. Student's *t* tests and Chi-squared tests were performed to determine the statistical significance of the difference in means between samples in the experiments reported in **Figures 2**,**4**,**5** and **Supplementary Figures 6** and **8**. $P < 0.05$ was considered statistically significant. Error bars represent s.e.m. No statistical methods were used to predetermine sample sizes, but these were similar to those employed in the field. We did not use randomization in this study, but for each experiment all genotypes were represented and appropriately blocked for data collection. We did not perform data collection and analysis blind to the conditions of the experiments because the properties of each cell type are so distinctive that the investigators would be able to tell the genotype of the animals by observation of the tissue sections. The data distribution was assumed to be normal, but this was not formally tested. Overall survival in **Figure 6** was assessed using the Kaplan-Meier survival analysis and the Mantel-Cox log-rank test was used to assess the significance of difference between survival curves. Data handling and statistical processing was performed using Microsoft Excel and Graphpad Prism Software.